Contents lists available at ScienceDirect

Journal of Alloys and Compounds

journal homepage: http://ees.elsevier.com

Dielectric properties of $CaCu_3Ti_4O_{12}$ ceramics doped with aluminium and fluorine

O.Z. Yanchevskii, O.I. V'yunov *, A.G. Belous, L.L. Kovalenko

V.I.Vernadsky Institute of General and Inorganic Chemistry NAS of Ukraine, Ukraine

ARTICLE INFO

Article history:
Received 7 October 2020
Received in revised form 22 March 2021
Accepted 5 April 2021
Available online xxx

Keywords
$CaCu_3Ti_4O_{12}$ ceramic
Complex dopant
Aluminium
Fluorine
Dielectric properties

ABSTRACT

The ceramics $CaCu_3Ti_{4-x}Al_xO_{12-0.5x-y}F_y$ were prepared using solid-state reactions technique and pre-synthesized $CaTiO_3$. It was found that the resistances of both the grain boundary R_{GB} and the interface between sample and electrode R_{SE} increase at the combined introduction of Al^{3+} and F^- ions. At 1100 °C, a decrease in dielectric properties after 12 h of sintering time due to copper losses was observed. The samples with x/y = 0.04/0.04 sintered for 10 h at 1 kHz are characterized by the following dielectric parameters: $\varepsilon' \approx 72{,}000$ and $\tan\delta \approx 0.047$. In the sample x/y = 0.04/0, the lowest dielectric loss ($\tan\delta \approx 0.044$) were found.

1. Introduction

Miniaturization of electronic devices is one of the tasks of modern microelectronics. In this regard, the development of materials with high ("colossal") dielectric constant ($\varepsilon' > 10^4$) and low dielectric loss ($\tan\delta < 0.05$) in a wide frequency and temperature range are of interest [1,2]. $CaCu_3Ti_4O_{12}$ (CCTO) is known to have a high dielectric constant ($\varepsilon' \approx 10^4$ in ceramics and thin films, and ~10^5 in single crystals) in a wide temperature (100–600 K) and frequency (1 Hz–10 MHz) ranges [3–5]. Various models explain the nature of high ε'. The internal barrier layers capacitance (IBLC) model assumes that the CCTO ceramics consists of high-conductive grains and non-conductive grain boundaries [4,6,7]. The surface barrier layers capacitance (SBLC) model takes into account the formation of the space charge regions near the electrodes [8,9]. Fang and Liu [10] directly observed internal domains and domain walls in $CaCu_3Ti_4O_{12}$ by electron microscopy. Earlier Subramanian et al. discovered the phenomenon of CCTO crystals twinning [11]. These facts allow the development of the nanoscale barrier layers capacitance (NBLC) model in the bulk of grains, where polarons exist within domains limited by plane defects [12].

$CaCu_3Ti_4O_{12}$ has the body-centred cubic perovskite structure ABO_3 with space group $Im\bar{3}m$ [3]. The Cu^{2+} and Ca^{2+} ions belong to A sublattice, but occupy crystallographic positions with different coordination (4 for Cu^{2+} and 12 for Ca^{2+}) due to the inclination of TiO_6 oxygen octahedra. In a real structure, the local disorder of Cu^{2+} and Ca^{2+} ions and the nanoscale disorder phases are possible [13], which increases the dynamic dielectric response. The disorder in single-crystal CCTO decreases with decreasing temperature and disappears at 100 K [14]. At the same temperature, the dielectric constant drop, and the large dielectric dispersion was observed [3].

The grain resistance CCTO depends on the number of weak-trapped electrons, which associated with the following n-type, or p-type transitions:

$$Cu^{2+} + e' \leftrightarrow Cu^{1+};\ Ti^{4+} + e' \leftrightarrow Ti^{3+};\ \text{or}\ Cu^{3+} + e' \leftrightarrow Cu^{2+}$$

In the temperature range of 150–350 K, the polaron electronic defects, in particular, the complex $Ti^{4+}O_5{\cdot}V^{\times}{}_O + e^-$ ($Ti^{4+}O_5{\cdot}V^{\bullet}{}_O$ or $Ti^{3+}O_5{\cdot}V^{\times}{}_O$) contribute to the conductivity. The conductivity arises due to electron transfer between $TiO_5{\cdot}V^{\bullet}{}_O$–$Cu'_{Cu}$ and $TiO_5{\cdot}V^{\times}{}_O$–$Cu^{\times}{}_{Cu}$ adjacent structures [12].

Copper ions have high thermal activity and at the sintering of CCTO ceramics leave their positions in the crystal lattice. This process changes the oxidative state of the remaining Cu^{2+} and Ti^{4+} ions [15–20]. The following mechanisms of defect formation are possible [17]:

$$3Cu^{2+} \rightarrow 2Cu^{1+} + Ti^{4+}{}_{Cu} + Cu\uparrow: \quad Ca(Cu^{2+}{}_{3-3v}Cu^{1+}{}_{2v}Ti^{4+}{}_v)Ti^{4+}{}_{4-v}O_{12} \qquad (1)$$

$$Cu^{+} + Ti^{4+} \rightarrow Cu^{2+} + Ti^{3+}{}_{Ti}: Ca(Cu^{2+}{}_{3-v}Ti^{4+}{}_v)Ti^{4+}{}_{4-2v}Ti^{3+}{}_{2v}O_{12} \qquad (2)$$

If sintering is prolonged, the following defect formation mechanism becomes dominant:

$$3Cu^{2+} \rightarrow V''{}_{Cu} + 2Cu^{3+} + Cu\uparrow: Ca(Cu^{2+}{}_{3-3v}Cu^{3+}{}_{2v}V''{}_v)Ti_4O_{12} \qquad (3)$$

* Corresponding author.
E-mail address: vyunov@ionc.kiev.ua (O.I. V'yunov)

https://doi.org/10.1016/j.jallcom.2021.159861
0925-8388/

During sintering at high temperatures, O^{2-} anions can also release from the crystal lattice, form neutral oxygen vacancies, and reduce the cations Cu^{2+}, Ti^{4+} [18]:

$$O^{2-}{}_O + 2Cu^{2+} \rightarrow \dot{V}_O + 2Cu^{1+} + 1/2O_2\uparrow: \quad Ca(Cu^{2+}{}_{3-u}Cu^{1+}{}_u)Ti^{4+}{}_4O_{12-u/2} \tag{4}$$

$$O^{2-}{}_O + 2Ti^{4+} \rightarrow \dot{V}_O + 2Ti^{3+} + 1/2O_2\uparrow: \quad CaCu^{2+}{}_3(Ti^{4+}{}_{4-w}Ti^{3+}{}_w)O_{12-w/2} \tag{5}$$

The decrease in the electrical resistance of grain of air-quenched CCTO ceramics confirms the significant impact of the oxygen vacancies in the conductivity formation [21].

Cu ions diffuse into the boundary layer results in the formation of Cu-rich area (Cu_xO-containing phases (CuO, Cu_4O_3, Cu_2O) or positively charged Cu ions) at intercrystalline grain boundaries and Cu vacancies at the domain boundaries . Cu vacancies at the domain boundaries form potential barriers for electron moving [19,22].

Thus, CCTO-based materials are sensitive to heat treatment conditions (temperatures, duration, sintering atmosphere) and to deviation from stoichiometry [17,23–25]. In order to improve CCTO characteristics, cation and anion substitutions were used [26–32]. The additions of Al^{3+} [33–39] and/or F^- [40–42] can affect the electrical characteristics of CCTO ceramics, but their role is not clearly understood. In this paper, we consider the effect of separate and combined additions of aluminium and fluorine on the dielectric properties of CCTO ceramics.

2. Experimental

Solid solutions with nominal composition $CaCu_3Ti_{4-x}Al_xO_{12-0.5x-y}F_y$ (where x/y = 0/0; 0.04/0; 0/0.04; 0.08/0; 0/0.08; 0.04/0.04; 0.08/0.08) were synthesized by solid-state reaction technique. Analytical grade CuC_2O_4, $CaCO_3$, CaF_2, $Al(NO_3)_3$, and extra pure grade TiO_2 (anatase) were used. At the first stage, $CaTiO_3$ was prepared from the stoichiometric mixture of $CaCO_3$ and TiO_2. Both reagents were previously dried for 4 h at 500 and 600 °C, respectively. Then they were milled in a vibrating mill using ZrO_2 balls and deionized water for 6 h. After drying at 100 °C, the mixture of $CaCO_3$ and TiO_2 heat-treated at 1100 °C for 6 h. At the second stage, stoichiometric mixtures of synthesised $CaTiO_3$, CuC_2O_4, TiO_2, CaF_2, and 1 M water solution of $Al(NO_3)_3$ were prepared. These mixtures were ground in a Retch PM100 planetary mill using ZrO_2 balls and isopropyl alcohol for 4 h at 300 rpm. Then, the mixtures were dried at 100 °C and double heat treated at 920 °C/12 h and 960 °C/12 h with intermediate grinding in an agate mortar with a pestle. The synthesized powders were mixed with a 5% aqueous solution of polyvinyl alcohol and passed through a 150 mesh nylon sieve. Disc-shaped specimens with a diameter of 8.5 mm and a thickness of 2 mm were pressed under a pressure of 120 MPa. Ceramics were sintered at 1100 °C for 10–12 h.

The phase composition of the products was determined by X-ray phase analysis (XRD) on a DRON-4-07 diffractometer (40 kV, 20 mA) using CuKα radiation and Ni filter. As certified standards, NIST SRM640e-SiO_2 (2Θ standard) and NIST SRM1976-Al_2O_3 (intensity standard) were used. The relative X-ray impulse counting error did not exceed 0.5%. The unit cell parameters of the samples were determined using FullProf software by the whole-pattern profile-matching Le Bail procedure [43]. The crystallite sizes of etched ceramic samples were studied using scanning electron microscope JEOL JEM-12301 and the average grain diameters were measured by at least 50 grains from different areas using ImageJ software [44]. The density of ceramics was determined by Archimedes principle.

To deposit the silver electrodes on polished ceramic samples, Ag-containing paste was burned at 600 °C for 0.5 h. The complex impedance of the samples with a diameter of 7.25 mm and a thickness of 1.6 mm was investigated using a 1260 Impedance/Gain-Phase Analyzer (Solartron Analytical). The equivalent circuit and the value of its components were determined using the ZView® software (Scribner Associates Inc., USA). Measurement error in the frequency range 10^3–10^5 Hz does not exceed 500 for ε′ and 0.002 for tan δ.

3. Results and discussion

Earlier we proposed the separate synthesis of CCTO components ($CaTiO_3$ and $CuTiO_3$) to avoid the formation of undesirable phases [45]. $CuTiO_3$ is not formed as a result of the eutectic reaction between CuO and TiO_2 from 500 to 1020 °C [46]. $CuTiO_3$ synthesized by the sol-gel method was no single phase [47]. We found that heat treatment of an equimolar mixture of CuC_2O_4 and TiO_2 at 600–900 °C for up to 12 h leads only phases of rutile and CuO. All these facts imply the thermodynamic instability of $CuTiO_3$.

XRD shows that after double (with intermediate grinding) heat treatments of the powder at 920–960 °C for at least 12 h, the single-phase solid solutions $CaCu_3Ti_{4-x}Al_xO_{12-0.5x-y}F_y$ are formed. Ceramic samples sintered at 1100 °C for 10 h matched the ICDD card 75–1149 and had space group $Im\bar{3}m$ (Fig. 1a). For Al-doped samples, the traces of copper oxides (Cu_2O, Cu_4O_3) arise due to the precipitation of the Cu-O secondary phase at grain boundaries of the ceramics surface layer [19,37].

The unit cell volume measured using the Le Bail method (Fig. 1b) at y = 0 (without fluorine), x = 0 (without aluminium), x = y (with an equal amount of aluminium and fluorine simultaneously) are shown in Fig. 2. A linear decrease in unit cell volume (V) from 404.08 Å^3 at x = 0 to 403.78 Å^3 at x = 0.08 (Fig. 2) indicates the formation of the $CaCu_3Ti_{4-x}Al_xO_{12-0.5x}$ solid solution. The unit cell volume decreases since Ti^{4+} ion (R = 0.605 Å) is replaced with a smaller Al^{3+} ion (R = 0.535 Å) [48]. In addition, to satisfy the electroneutrality condition, a

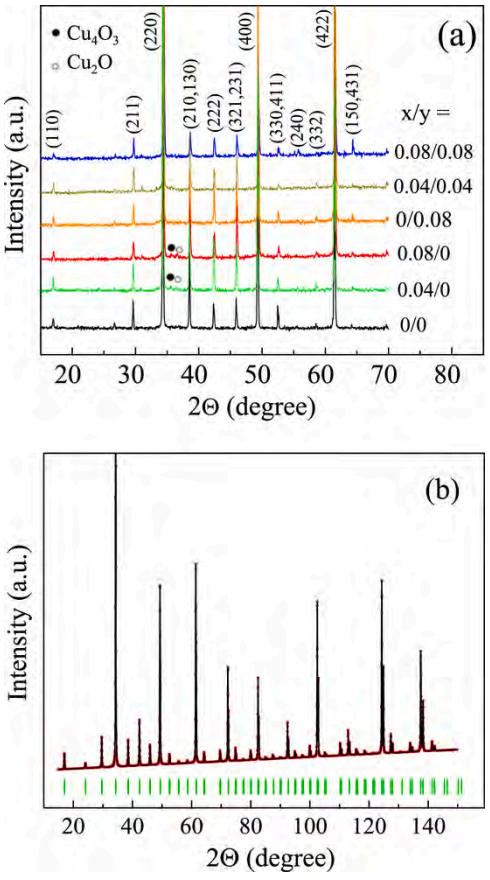

Fig. 1. (a) XRPD patterns of ceramic samples $CaCu_3Ti_{4-x}Al_xO_{12-0.5x-y}F_y$, sintered at 1100 °C for 10 h; (b) experimental (dots) and calculated (line) room-temperature XRPD pattern of ceramic x/y = 0.08/0.08. Bars show the peak positions.

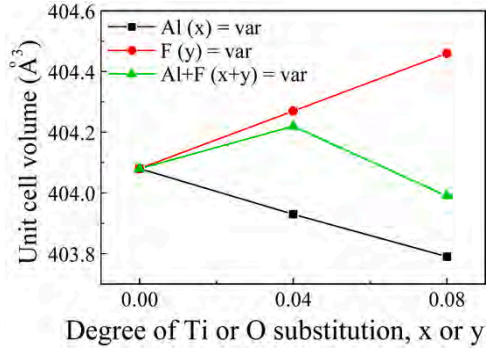

Fig. 2. Concentration dependences of the unit cell volume for ceramic samples $CaCu_3Ti_{4-x}Al_xO_{12-0.5x-y}F_y$, sintered at 1100 °C for 10 h.

decrease in the charge of B sublattice of ABO_3 perovskite structure should be compensated by an increase in the charge of the A-sublattice due to a decrease in the number of Cu^{1+} ions. When an Al-containing compound was added to pre-synthesized CCTO particles, a core-shell structure with Al_2O_3 outside was formed [36]. Therefore, substitutions $Al^{3+} \rightarrow Ti^{4+}$ in CCTO occur only at the synthesis stage: at 700–750 °C chemically inert Al_2O_3 react with CuO to form the intermediate compound $CuAl_2O_4$ [49].

In $CaCu_3Ti_4O_{12-y}F_y$ system, the substitution of O^{2-} (R = 1.40 Å) by F^- ions (R = 1.33 Å) [48] results in V increase (Fig. 2) from 404.08 Å^3 (y = 0) to 404.46 Å^3 (y = 0.08). This fact can be explained by the appearance of large ions Cu^{1+} ($R_{Cu}{}^{1+}$ = 0.60 Å > $R_{Cu}{}^{2+}$ = 0.57 Å) and Ti^{3+} ($R_{Ti}{}^{3+}$ = 0.67 Å > $R_{Ti}{}^{4+}$ = 0.605 Å) due to the reduction of the Cu^{2+} and/or Ti^{4+} [48]. The difference in ionic radii of O^{2-} and F^- is insignificant and the appearance of Cu^{1+} and Ti^{3+} ions is the key factor increasing the unit cell volume. In this case, solid solutions can be written as $Ca(Cu^{2+}{}_{3-y}Cu^{1+}{}_y)Ti_4O_{12-y}F_y$ or $CaCu^{2+}{}_3(Ti^{4+}{}_{4-y}Ti^{3+}{}_y)O_{12-y}F_y$ respectively.

In the system $CaCu_3Ti_{4-x}Al_xO_{12-0.5x-y}F_y$ (Fig. 2), the change in V additively depends on the contributions of Al^{3+} and F^- additives (x and y values respectively). At low degrees of doping (x/y = 0.04/0.04), the unit cell volume increases as expected. At a high degree of doping (x/y = 0.08/0.08), a decrease in the unit cell volume to 403.99 Å^3 indicates a decrease in the content of Cu^{1+} and Ti^{3+} ions in the grains. Substitutions at Ti^{4+} and O^{2-} positions differently affect the relative density of the $\rho_{exper}/\rho_{theor}$ of $CaCu_3Ti_{4-x}Al_xO_{12-0.5x-y}F_y$ ceramic. In Al-containing system, the ceramic density monotonically decreases from 95.5% to 96% (x = 0) to 91–90% (x = 0.08) with the degree of substitution and increases with the sintering time (Fig. 3a). In the F-containing system, the ceramic density slightly decreases both with the degree of substitution and with the sintering time from 95% to 94% (Fig. 2b). An increase in the sintering time or temperature results in similar phenomena, namely, additional copper losses and an increase in the number of voids.

Fig. 4 shows the microstructure of $CaCu_3Ti_{4-x}Al_xO_{12-0.5x-y}F_y$ ceramics. The average ceramic grain size is 1.5(5) μm at x/y = 0/0 (Fig. 4a); 4(1) μm at x/y = 0.08/0 (Fig. 4b). A bimodal structure with small, 2.5(5) μm and large, 10(2) μm grains is observed at x/y = 0/0.08 (Fig. 4c). The largest grains of 125(25) μm are observed at x/y = 0.08/0.08 (Fig. 4d). Obviously, the addition of both Al^{3+} and F^- ions in CCTO structure promotes grain growth. The simultaneous introduction of aluminium and fluorine leads to an abnormal grain growth, which indicates a synergistic effect. The reason for the abnormal grain growth in $CaCu_3Ti_{4-x}Al_xO_{12-0.5x-y}F_y$ ceramics may be a presence of liquid phase at the grain boundaries. The liquid phase at the grain boundaries promotes interface migration. In this case, the size distribution of ceramic grains is bimodal [50]. A liquid phase is probably formed as a eutectic in a complex system Cu–Al–Ti–F–O. This assumption is supported by the fact that a liquid phase occurs in the known oxide systems at temperatures below 1100 °C, namely: 919 °C (CuO-TiO_2) [46] and 740–750 °C (CuF_2-Cu_2O-CuO) [51]. The release of copper from grains and segregation at grain boundaries with the formation of low-melting eutectics is also confirmed by a decrease in the unit cell volume for the sample with x/y = 0.08/0.08 (Fig. 2).

Fig. 5 shows Cole-Cole diagrams of the complex impedance of the ceramic samples $CaCu_3Ti_{4-x}Al_xO_{12-0.5x-y}F_y$ at room temperature. The diagram for sample $x/y = 0/0$ consists of two spaced in frequency semicircles that indicate two relaxation mechanisms in electrically inhomogeneous phases. The diagrams for other samples contains the distorted semicircles, the size of which increases in the series: $x/y = 0/0 < x/y = 0.04/0.04 < x/y = 0/0.08 < x/y = 0.04/0 < x/y = 0.08/0 < x/y = 0.08/0.08$. The equivalent circuit for the complex impedance of $CaCu_3Ti_{4-x}Al_xO_{12-0.5x-y}F_y$ ceramics (Fig. 5, insert) is composed of resistance R_G and two series linked subcircuits with a parallel-connected resistor and constant phase element (CPE) [9,52,53]. Subscripts show elements belonging to grain (G), grain boundary (GB), and the interface between sample and electrode (SE). The CPE constant phase element describes the electrical inhomogeneity of phases (due to chemical or size inhomogeneity) according to the following formula [53]:

$$Z_{CPE} = A^{-1} (i\omega)^{-n} \quad (6)$$

where A is the proportionality factor, the dimension of which depends on the exponent n; i is the imaginary unit, ω is the angular frequency of the alternating current. At n = 1 and in the vicinity, the CPE is identical to the distributed capacitor and at n = 0.5 and in the vicinity, the CPE is identical to the Warburg element.

The parameters of the equivalent circuit of the samples were determined by fitting the experimental dependence $Z'' = f(Z')$ (Table 1). Table 1 shows that the addition of aluminium and fluorine respectively increases and slightly decreases the electrical resistance of the grain R_G.

The monotonic increase in R_G of the ceramics of the system $CaCu_3Ti_{4-x}Al_xO_{12-0.5x}$ with the aluminium content (Table 1) indicates the number of Cu^{1+} and Ti^{3+} forming due to Eqs. (1), (2) decreases.

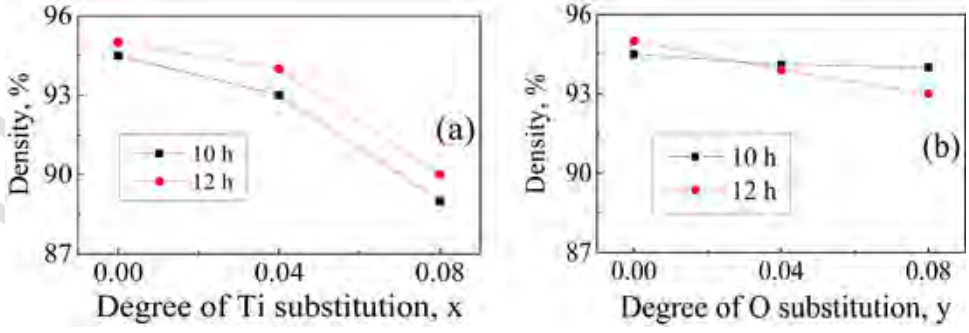

Fig. 3. The relative density of ceramics $CaCu_3Ti_{4-x}Al_xO_{12-0.5x}$ (a) and $CaCu_3Ti_4O_{12-y}F_y$ (b), sintered at 1100 °C.

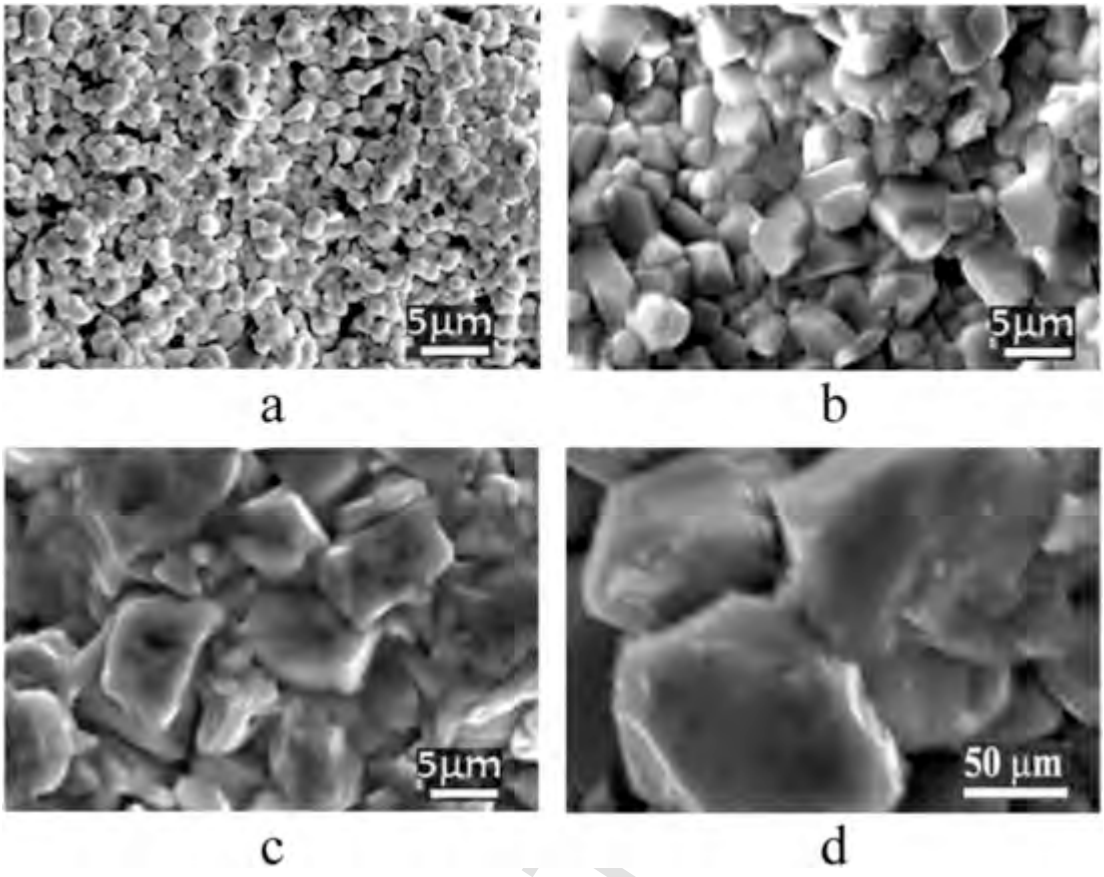

Fig. 4. The microstructure of ceramic samples $CaCu_3Ti_{4-x}Al_xO_{12-0.5x-y}F_y$, sintered at 1100 °C for 10 h: $x/y = 0/0$ (a); $x/y = 0.08/0$ (b); $x/y = 0/0.08$ (c); $x/y = 0.08/0.08$ (d).

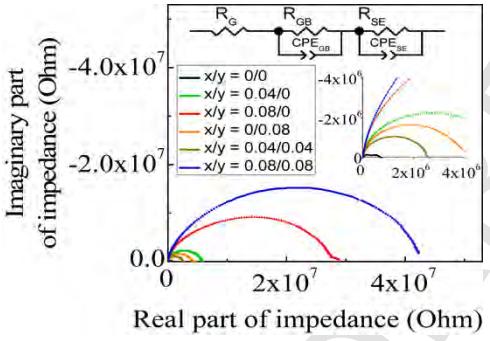

Fig. 5. Complex impedance diagrams at room temperature and an equivalent circuit (insert) for ceramic samples $CaCu_3Ti_{4-x}Al_xO_{12-0.5x-y}F_y$, sintered at 1100 °C for 10 h. R and CPE are resistance and a constant phase element. Subscripts show grain (G), grain boundary (GB) and the interface between sample and electrode (SE).

However, the significant increase in R_G cannot be explained only by the proportional decrease in the number of reduced cations, because the concentration of Al^{3+} ions in the Ti^{4+} positions is ≤2%. At the same time, the formation of solid solution $CaCu_3Ti_{4-x}Al_xO_{12-0.5x}$ is accompanied by the appearance of oxygen vacancies. These oxygen vacancies form $Al^{3+}O_5{\cdot}V^{\times}{}_O$ clusters that cannot participate in polaron charge transfer but have a competitive advantage over the formation of conducting polarons $Ti^{3+}O_5{\cdot}V^{\times}{}_O$ [12]. This fact can explain the significant increase in R_G with the increase of Al content.

In contrast to aluminium-doped CCTO, in fluorine-doped one, the ions in lower oxidation states are formed not only at the sintering stage, but already at the synthesis stage. The reasons for Cu^{2+} and Ti^{4+} reduction in $CaCu_3Ti_4O_{12-y}F_y$ is the charge compensation requirements for the formation of solid solutions $Ca(Cu^{2+}{}_{3-y}Cu^{1+}{}_y)Ti^{4+}{}_4O_{12-y}F_y$ and $CaCu^{2+}{}_3(Ti^{4+}{}_{4-y}Ti^{3+}{}_y)O_{12-y}F_y$. Thus, it can be expected that the resistance of the grain will increase in order $R_G(CaCu_3Ti_4O_{12-y}F_y) < R_G(CaCu_3Ti_4O_{12}) < R_G(CaCu_3Ti_{4-x}Al_xO_{12-0.5x})$. However, really the resistance of the grains of $CaCu_3Ti_4O_{12-y}F_y$ decreases insignificantly. This fact can be explained by an increase in fluorine segregation with an increase in y and the formation of low-melting (740–750 °C) CuF_2 – Cu_2O – CuO eutectics [51]. Therefore, this part of fluorine does not participate in the formation of a solid solution and does not contribute to the reduction of Cu^{2+} and Ti^{4+} cations.

The addition of aluminium and fluorine significantly, by order of magnitude and more, increases the resistance of the grain boundary R_{GB} and of the interface between sample and electrode R_{SE} (Table 1). The resistance of grain R_G increases due to an increase in the aluminium content for the reasons described above. The increase in the R_{GB} and R_{SE} can be explained by the segregation of copper-containing phases (Cu_xO, $x \leq 1$) in these regions. The electrical resistance of these phases is several orders of magnitude higher than CCTO [54]. In addition, due to abnormal grain growth in aluminium- and fluorine-doped ceramic, the surface of grain boundaries decreases sharply, and the surface density of Cu_xO phases increases.

The increase in the duration of ceramics sintering from 10 to 12 h increases the values of R_G, R_{GB}, and R_{SE} (Table 1). This can be explained by the fact that the dominant mechanism of defect formation changes with time from (1) to (3). In this case, mutual compensation of Cu^+/Ti^{3+} and Cu^{3+} ions occurs:

$$Cu^{3+} + Cu^{1+} \rightarrow 2Cu^{2+} \quad (7)$$

$$Cu^{3+} + Ti^{3+} \rightarrow Cu^{2+} + Ti^{4+} \quad (8)$$

Eqs. (7), (8) shows that with long sintering, the number of charge carriers decreases, and R_G increases. An increase in sintering time is ac-

Table 1
Equivalent circuit elements parameters for ceramic samples $CaCu_3Ti_{4-x}Al_xO_{12-0.5x-y}F_y$, sintered at 1100 °C for 10 and 12 h.

x/y	Sinter. time, h	Grain	Grain boundary			Interface sample/electrode		
		R_G, Ω	R_{GB}, Ω	C_{GB}, F	n_{GB}	R_{SE}, Ω	C_{SE}, F	n_{SE}
0/0	10	22(4)	3.8(2) × 10^{5}	3.3(3) × 10^{-9}	0.802(4)	3.1(1) × 10^{5}	3.3(1) × 10^{-8}	0.905(3)
	12	24(2)	5.5(3) × 10^{5}	1.2(5) × 10^{-9}	0.791(2)	6.4(3) × 10^{5}	2.8(5) × 10^{-8}	0.917(2)
0.04/0	10	37(2)	2.3(1) × 10^{5}	2.2(1) × 10^{-9}	0.968(6)	3.2(1) × 10^{5}	8.1(5) × 10^{-8}	0.885(3)
	12	46(3)	5.4(3) × 10^{5}	2.4(4) × 10^{-9}	0.930(5)	5.6(2) × 10^{5}	6.6(7) × 10^{-8}	0.898(4)
0.08/0	10	58(7)	3.1(2) × 10^{5}	4.6(5) × 10^{-9}	0.803(2)	5.4(2) × 10^{5}	4.2(1) × 10^{-9}	0.980(9)
	12	70(7)	3.9(2) × 10^{5}	3.4(2) × 10^{-9}	0.862(3)	1.2(2) × 10^{5}	2.2(1) × 10^{-9}	0.993(5)
0/0.08	10	19(4)	1.2(2) × 10^{5}	5.7(6) × 10^{-9}	0.818(9)	5.0(3) × 10^{5}	2.3(1) × 10^{-8}	0.935(3)
	12	22(5)	7.1(1) × 10^{5}	2.2(1) × 10^{-9}	0.793(7)	1.1(1) × 10^{6}	3.6(1) × 10^{-9}	0.971(2)
0.04/0.04	10	26(5)	2.6(3 × 10^{6}	3.3(5) × 10^{-9}	0.978(5)	8.0(2) × 10^{5}	3.1(1) × 10^{-7}	0.903(2)
	12	32(3)	4.9(4) × 10^{6}	2.7(7) × 10^{-9}	0.932(5)	1.8(2) × 10^{6}	6.2(5) × 10^{-7}	0.919(4)
0.08/0.08	10	42(4)	4.3(3) × 10^{6}	1.6(5) × 10^{-9}	0.924(4)	2.4(2) × 10^{6}	2.1(5) × 10^{-8}	0.876(5)
	12	47(5)	9.8(5) × 10^{6}	2.4(2) × 10^{-9}	0.908(5)	7.2(2) × 10^{6}	4.6(7) × 10^{-8}	0.891(3)

companied by further segregation of copper and the formation of copper-containing phases at grain boundaries, which increases R_{GB} and R_{SE}.

Fig. 6 and Table 2 show the frequency dependences of ε′ and tan δ at room temperature of the ceramic $CaCu_3Ti_{4-x}Al_xO_{12-0.5x-y}F_y$ sintered at 1100 °C/10 h. All samples except x/y = 0.08/0 have high permittivity ε′ > 30,000 in a wide frequency range (Fig. 6a). It should be noted that only aluminium at a low degree of substitution (x ≤ 0.04) increases the dielectric constant of the solid solution as compared to CCTO. The value ε′ increases only with joint doping when x/y = 0.04/0.04. The dielectric properties of pure CCTO ceramics differ markedly from the doped ones (Fig. 6). At ultra-low frequencies, strong relaxation and high values of $\varepsilon' > 10^6$ are observed. Low-frequency relaxation is probably observed because of the interfacial polarization contribution of electrically inhomogeneous phases. Both aluminium and fluorine dopants suppress the contribution of interfacial polarization of CCTO ceramic at ultra-low frequencies and extend the range of low dielectric losses towards low frequencies. In addition, dielectric losses are significantly decreased (Fig. 6b). Despite the increase in the density of $CaCu_3Ti_{4-x}Al_xO_{12-0.5x-y}F_y$ ceramics with an increase in sintering time from 10 h to 12 h (Fig. 3), its dielectric constant decreases and dielectric losses increase (Table 2). This may be due to excess copper losses and, accordingly, a decrease in the number of Cu^{1+} and Ti^{3+} ions in the grains. The composition with x/y = 0.04/0 at room temperature and 1 kHz has the lowest dielectric loss (tan δ ≈ 0.044). The composition with x/y = 0.04/0.04 has the best combination of dielectric characteristics: ε′ ≈ 72,000, tan δ ≈ 0.047. These characteristics are comparable or higher than known ones for Al_2O_3-modified CCTO ceramics (ε′ ≈ 43,000, tan δ ≈ 0.06 [37], ε′ ≈ 81,000, tan δ ≈ 0.08 [36]) or F-modified CCTO ceramics (ε′ ≈ 81,000, tan δ ≈ 0.077 [41]).

4. Conclusions

Ceramics of the system $CaCu_3Ti_{4-x}Al_xO_{12-y}F_y$ were prepared by solid-state reactions technique that involves the preliminary synthesis of $CaTiO_3$. The ability to use CaF_2 as a fluorine source was shown. The combined introduction of aluminium and fluorine ions results in synergetic abnormal grain growth due to the formation of a liquid phase at grain boundaries. The liquid phase is supposed to form as a eutectic in a complex system Cu–Al–Ti–F–O.

In the system $CaCu_3Ti_{4-x}Al_xO_{12-0.5x}$, the resistance of grains monotonically increases with x. In the system $CaCu_3Ti_4O_{12-y}F_y$, the difference between the grain resistance of doped and undoped samples in the system $CaCu_3Ti_4O_{12-y}F_y$ is small. The ceramic sample $CaCu_3Ti_{4-x}Al_xO_{12-y}F_y$ with x/y = 0.04/0.04 after sintering for 10 h has the following dielectric parameters: ε′ ≈ 71,000 (1 kHz) and tan δ ≈ 0.047.

CRediT authorship contribution statement

O.Z. Yanchevskii: Methodology, Resources, Writing - original draft. **O.I. V'yunov:** Conceptualization, Investigation, Writing - origi-

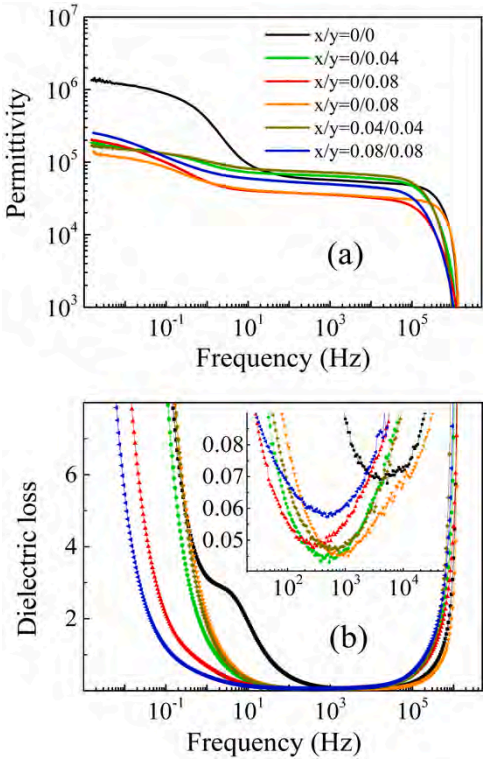

Fig. 6. Frequency dependences of permittivity ε′ (a) and dielectric loss tan δ (b) at room temperature for ceramic samples $CaCu_3Ti_{4-x}Al_xO_{12-0.5x-y}F_y$, sintered at 1100 °C for 10 h.

Table 2
Dielectric characteristics of ceramic samples $CaCu_3Ti_{4-x}Al_xO_{12-0.5x-y}F_y$, sintered at 1100 °C for 10 and 12 h.

x/y	Sintering time, h	Permittivity, ε′		Dielectric loss, tan δ	
		at 1 kHz	at 100 kHz	at 1 kHz	min value
0/0	10	57,000	47,000	0.088	0.070
	12	46,000	38,000	0.098	0.068
0.04/0	10	63,500	47,000	0.047	0.044
	12	50,000	40,000	0.066	0.066
0.08/0	10	36,000	24,000	0.055	0.048
	12	32,000	25,000	0.065	0.056
0/0.08	10	36,000	31,000	0.046	0.046
	12	23,500	19,500	0.058	0.058
0.04/0.04	10	72,000	53,000	0.047	0.047
	12	66,800	48,300	0.057	0.055
0.08/0.08	10	50,000	32,600	0.060	0.057
	12	43,000	26,200	0.077	0.072

nal draft. **A.G. Belous:** Supervision, Validation. **L.L. Kovalenko:** Investigation, Data curation.

Declaration of Competing Interest

The authors declare that they have no known competing financial interests or personal relationships that could have appeared to influence the work reported in this paper.

Acknowledgments

This work was supported by the Research program of the Ukrainian National Academy of Sciences "New functional substances and materials for chemical production" (Fine Chemicals) [grant number 0119U101351].

References

[1] A.I. Kingon, J.-P. Maria, S.K. Streiffer, Alternative dielectrics to silicon dioxide for memory and logic devices, Nature 406 (2000) 1032–1038, doi:10.1038/35023243.
[2] U.S. Congress, Office of Technology Assessment, Miniaturization Technologies, OTA-TCT514, Government Printing Office, Washington, DC, U.S., (1991).
[3] M.A. Subramanian, D. Li, N. Duan, B.A. Reisner, A.W. Sleight, High dielectric constant in $ACu_3Ti_4O_{12}$ and $ACu_3Ti_3FeO_{12}$ phases, J. Solid State Chem. 151 (2000) 323–325, doi:10.1006/jssc.2000.8703.
[4] L.C. Kretly, A.F.L. Almeida, R.S. De Oliveira, J.M. Sasaki, A.S.B. Sombra, Electrical and optical properties of $CaCu_3Ti_4O_{12}$ (CCTO) substrates for microwave devices and antennas, Microw. Opt. Technol. Lett. 39 (2003) 145–150, doi:10.1002/mop.11152.
[5] R. Löhnert, H. Bartsch, R. Schmidt, B. Capraro, J. Töpfer, Microstructure and electric properties of $CaCu_3Ti_4O_{12}$ multilayer capacitors, J. Am. Ceram. Soc. 98 (2015) 141–147, doi:10.1111/jace.13260.
[6] B.K. Kim, H.S. Lee, J.W. Lee, S.E. Lee, Y.S. Cho, Dielectric and grain-boundary characteristics of hot pressed $CaCu_3Ti_4O_{12}$, J. Am. Ceram. Soc. 93 (2010) 2419–2422, doi:10.1111/j.1551-2916.2010.03738.x.
[7] V. Brizé, G. Gruener, J. Wolfman, K. Fatyeyeva, M. Tabellout, M. Gervais, F. Gervais, Grain size effects on the dielectric constant of $CaCu_3Ti_4O_{12}$ ceramics, Mater. Sci. Eng. B 129 (2006) 135–138, doi:10.1016/j.mseb.2006.01.004.
[8] G. Deng, T. Yamada, P. Muralt, Evidence for the existence of a metal-insulator-semiconductor junction at the electrode interfaces of $CaCu_3Ti_4O_{12}$ thin film capacitors, Appl. Phys. Lett. 91 (2007) 202903, doi:10.1063/1.2814043.
[9] P. Lunkenheimer, R. Fichtl, S.G. Ebbinghaus, A. Loidl, Nonintrinsic origin of the colossal dielectric constants in $CaCu_3Ti_4O_{12}$, Phys. Rev. B 70 (2004) 172102, doi:10.1103/PhysRevB.70.172102.
[10] T.-T. Fang, C. Liu, Evidence of the internal domains for inducing the anomalously high dielectric constant of $CaCu_3Ti_4O_{12}$, Chem. Mater. 17 (2005) 5167–5171, doi:10.1021/cm051180k.
[11] M.A. Subramanian, A.W. Sleight, $ACu_3Ti_4O_{12}$ and $ACu_3Ru_4O_{12}$ perovskites: high dielectric constants and valence degeneracy, Solid State Sci. 4 (2002) 347–351, doi:10.1016/S1293-2558(01)01262-6.
[12] P.R. Bueno, R. Tararan, R. Parra, E. Joanni, M.A. Ramirez, W.C. Ribeiro, E. Longo, J.A. Varela, A polaronic stacking fault defect model for $CaCu_3Ti_4O_{12}$ material: an approach for the origin of the huge dielectric constant and semiconducting coexistent features, J. Phys. D Appl. Phys. 42 (2009) 055404, doi:10.1088/0022-3727/42/5/055404.
[13] Y. Zhu, J.C. Zheng, L. Wu, A.I. Frenkel, J. Hanson, P. Northrup, W. Ku, Nanoscale disorder in $CaCu_3Ti_4O_{12}$: a new route to the enhanced dielectric response, Phys. Rev. Lett. 99 (2007) 037602, doi:10.1103/PhysRevLett.99.037602.
[14] T. Hori, M. Takesada, A. Onodera, Structural aspects in A-site ordered perovskite $CaCu_3Ti_4O_{12}$: colossal dielectric behavior and Ca/Cu disordering, Ferroelectrics 513 (2017) 72–77, doi:10.1080/00150193.2017.1350500.
[15] R. Schmidt, M.C. Stennett, N.C. Hyatt, J. Pokorny, J. Prado-Gonjal, M. Li, D.C. Sinclair, Effects of sintering temperature on the internal barrier layer capacitor (IBLC) structure in $CaCu_3Ti_4O_{12}$ (CCTO) ceramics, J. Eur. Ceram. Soc. 32 (2012) 3313–3323, doi:10.1016/j.jeurceramsoc.2012.03.040.
[16] J.J. Romero, P. Leret, F. Rubio-Marcos, A. Quesada, J.F. Fernández, Evolution of the intergranular phase during sintering of $CaCu_3Ti_4O_{12}$ ceramics, J. Eur. Ceram. Soc. 30 (2010) 737–742, doi:10.1016/j.jeurceramsoc.2009.08.024.
[17] R. Schmidt, S. Pandey, P. Fiorenza, D.C. Sinclair, Non-stoichiometry in "$CaCu_3Ti_4O_{12}$" (CCTO) ceramics, RSC Adv. 3 (2013) 14580–14589, doi:10.1039/C3RA41319E.
[18] T.-T. Fang, Elements of Structures and Defects of Crystalline Materials, Elsevier, 2018.
[19] W.-X. Yuan, Z. Luo, C. Wang, Investigation on effects of CuO secondary phase on dielectric properties of $CaCu_3Ti_4O_{12}$ ceramics, J. Alloy. Compd. 562 (2013) 1–4, doi:10.1016/j.jallcom.2013.02.035.
[20] Y. Chen, Y. Teng, X. Zhao, L. Wu, Effect of synthesis process on CuO segregation and dielectric properties of $CaCu_3Ti_4O_{12}$ ceramic, J. Wuhan Univ. Technol. Mater. Sci. Ed. 34 (2019) 1089–1096, doi:10.1007/s11595-019-2164-1.
[21] W. Li, L. Tang, F. Xue, Z. Xin, Z. Luo, G. Du, Large reduction of dielectric losses of $CaCu_3Ti_4O_{12}$ ceramics via air quenching, Ceram. Int. 43 (2017) 6618–6621, doi:10.1016/j.ceramint.2017.02.029.
[22] T.-T. Fang, K.-T. Lee, New insights into understanding the defect structures and relationship of frequency dependences of dielectric permittivity and ac conductivity of $CaCu_3Ti_4O_{12}$, J. Appl. Phys. 125 (2019) 215106, doi:10.1063/1.5086328.
[23] J. Zhao, H. Zhao, Z. Zhu, Influence of sintering conditions and CuO loss on dielectric properties of $CaCu_3Ti_4O_{12}$ ceramics, Mater. Res. Bull. 113 (2019) 97–101, doi:10.1016/j.materresbull.2019.01.014.
[24] S. Kumar, N. Ahlawat, N. Ahlawat, Effect of heating rate on microstructure and electrical properties of microwave sintered $CaCu_3Ti_4O_{12}$ ceramics, Adv. Mater. Lett. 8 (2017) 605–613, doi:10.5185/amlett.2017.6398.

[25] P. Liu, Y. Lai, Y. Zeng, S. Wu, Z. Huang, J. Han, Influence of sintering conditions on microstructure and electrical properties of $CaCu_3Ti_4O_{12}$ (CCTO) ceramics, J. Alloy. Compd. 650 (2015) 59–64, doi:10.1016/j.jallcom.2015.07.247.
[26] L. Singh, U.S. Rai, K.D. Mandal, M. Yashpal, Dielectric properties of ultrafine Zn-doped $CaCu_3Ti_4O_{12}$ ceramic, J. Adv. Dielectr. 02 (2012) (1250007-1250006), doi:10.1142/S2010135X12500075.
[27] Z. Yang, Y. Zhang, G. You, K. Zhang, R. Xiong, J. Shi, Dielectric and electrical transport properties of the Fe^{3+}-doped $CaCu_3Ti_4O_{12}$, J. Mater. Sci. Technol. 28 (2012) 1145–1150, doi:10.1016/S1005-0302(12)60184-4.
[28] F. Luo, J. He, J. Hu, Y.H. Lin, Electric and dielectric behaviors of Y-doped calcium copper titanate, J. Am. Ceram. Soc. 93 (2010) 3043–3045, doi:10.1111/j.1551-2916.2010.04022.x.
[29] S. Jin, H. Xia, Y. Zhang, Effect of La-doping on the properties of $CaCu_3Ti_4O_{12}$ dielectric ceramics, Ceram. Int. 35 (2009) 309–313, doi:10.1016/j.ceramint.2007.10.007.
[30] W. Li, S. Qiu, N. Chen, G. Du, Enhanced dielectric response in Mg-doped $CaCu_3Ti_4O_{12}$ ceramics, J. Mater. Sci. Technol. 26 (2010) 682–686, doi:10.1016/S1005-0302(10)60107-7.
[31] M. Ahmadipour, M.F. Ain, Z.A. Ahmad, A short review on copper calcium titanate (CCTO) electroceramic: synthesis, dielectric properties, film deposition, and sensing application, Nano Micro Lett. 8 (2016) 291–311, doi:10.1007/s40820-016-0089-1.
[32] S. Kawrani, M. Boulos, D. Cornu, M. Bechelany, From synthesis to applications: copper calcium titanate (CCTO) and its magnetic and photocatalytic properties, ChemistryOpen 8 (2019) 922–950, doi:10.1002/open.201900133.
[33] S.W. Choi, S.H. Hong, Y.M. Kim, Effect of Al doping on the electric and dielectric properties of $CaCu_3Ti_4O_{12}$, J. Am. Ceram. Soc. 90 (2007) 4009–4011, doi:10.1111/j.1551-2916.2007.01983.x.
[34] L. Shengtao, W. Hui, L. Chunjiang, Y. Yang, L. Jianying, Dielectric properites of Al-doped $CaCu_3Ti_4O_{12}$ ceramics by coprecipitation method, in: Proceedings of 2011 International Symposium on Electrical Insulating Materials, IEEE, 2011, pp. 23-26. doi: 10.1109/ISEIM.2011.6826267.
[35] J. Boonlakhorn, P. Kidkhunthod, N. Chanlek, P. Thongbai, (Al^{3+}, Nb^{5+}) co–doped $CaCu_3Ti_4O_{12}$: an extended approach for acceptor–donor heteroatomic substitutions to achieve high–performance giant–dielectric permittivity, J. Eur. Ceram. Soc. 38 (2018) 137–143, doi:10.1016/j.jeurceramsoc.2017.08.040.
[36] S. De Almeida-Didry, M.M. Nomel, C. Autret, C. Honstettre, A. Lucas, F. Pacreau, F. Gervais, Control of grain boundary in alumina doped CCTO showing colossal permittivity by core-shell approach, J. Eur. Ceram. Soc. 38 (2018) 3182–3187, doi:10.1016/j.jeurceramsoc.2018.03.003.
[37] Y. Zhang, L.L. Xue, K. Zeng, X.W. Wang, L.Y. Sun, X.H. Meng, Y.C. Shi, Y.Y. Li, M.Z. Cao, Y.C. Hu, Dielectric properties of Al_2O_3 modified $CaCu_3Ti_4O_{12}$ ceramics, J. Mater. Sci. Mater. Electron. 30 (2019) 13869–13876, doi:10.1007/s10854-019-01810-2.
[38] K. Pal, A. Dey, R. Jana, P.P. Ray, P. Bera, L. Kumar, T.K. Mandal, P. Mohanty, M.M. Seikh, A. Gayen, Citrate combustion synthesized Al-doped $CaCu_3Ti_4O_{12}$ quadruple perovskite: synthesis, characterization and multifunctional properties, PCCP, 22, (2020) 3499–3511. doi: ⟨10.1039/C9CP05005A⟩.
[39] J. Jumpatam, N. Chanlek, P. Thongbai, Giant dielectric response, electrical properties and nonlinear current-voltage characteristic of Al_2O_3-$CaCu_3Ti_4O_{12}$ nanocomposites, Appl. Surf. Sci. 476 (2019) 623–631, doi:10.1016/j.apsusc.2019.01.136.
[40] A.E. Smith, T.G. Calvarese, A.W. Sleight, M.A. Subramanian, An anion substitution route to low loss colossal dielectric $CaCu_3Ti_4O_{12}$, J. Solid State Chem. 182 (2009) 409–411, doi:10.1016/j.jssc.2008.10.037.
[41] J. Jumpatam, B. Putasaeng, N. Chanlek, P. Kidkhunthod, P. Thongbai, S. Maensiri, P. Chindaprasirt, Improved giant dielectric properties of $CaCu_3Ti_4O_{12}$ via simultaneously tuning the electrical properties of grains and grain boundaries by F– substitution, RSC Adv. 7 (2017) 4092–4101, doi:10.1039/C6RA27381E.
[42] J. Jumpatam, N. Chanlek, M. Takesada, P. Thongbai, Giant dielectric behavior of monovalent cation/anion (Li+, F–) co-doped $CaCu_3Ti_4O_{12}$ ceramics, J. Am. Ceram. Soc. 103 (2020) 1871–1880, doi:10.1111/jace.16904.
[43] A. Le Bail, Whole powder pattern decomposition methods and applications: a retrospection, Powder Diffr. 20 (2005) 316–326, doi:10.1154/1.2135315.
[44] AENOR, ISO 13383–1:2016 Fine ceramics (advanced ceramics, advanced technical ceramics) - Microstructural characterization - Part 1: Determination of grain size and size distribution (ISO 13383–1:2012), International Organization for Standardization, Geneva, Switzerland, (2016), pp. 29.
[45] O.I. V'yunov, B.A. Konchus, O.Z. Yanchevskiy, A.G. Belous, Synthesis, properties $CaCu_3Ti_4O_{12}$ with colossal value of the dielectric permittivity, Ukr. Chem. J. 85 (2019) 77–86, doi:10.33609/0041-6045.85.6.2019.77-86.
[46] F.-H. Lu, F.-X. Fang, Y.-S. Chen, Eutectic reaction between copper oxide and titanium dioxide, J. Eur. Ceram. Soc. 21 (2001) 1093–1099, doi:10.1016/S0955-2219(00)00298-3.
[47] G.A. Traistaru, C.I. Covaliu, O. Oprea, V. Matei, D. Matei, D.L. Cursaru, I. Jitaru, $MTiO_3$ (M = Cu, Ni) as catalysts in toluene oxidation, Rev. Chim. 62 (2011) 773–776.
[48] R.D. Shannon, Revised effective ionic radii and systematic studies of interatomic distances in halides and chalcogenides, Acta Crystallogr. Sect. A Cryst. Phys. Diffr. Theor. Gen. Crystallogr. 32 (1976) 751–767, doi:10.1107/S0567739476001551.
[49] N. Wolff, D. Klimm, D. Siche, Thermodynamic investigations on the growth of $CuAlO_2$ delafossite crystals, J. Solid State Chem. 258 (2018) 495–500, doi:10.1016/j.jssc.2017.11.014.
[50] S.-J.L. Kang, Sintering: Densification, Grain Growth and Microstructure, Elsevier Butterworth-Heinemann, Oxford, 2004.
[51] F. Deschênes-Allard, C. Robelin, D. Zanghi, S. Bouvet, S. Ory, E. Véron, K. Machado, C. Bessada, P. Chartrand, Experimental and thermodynamic assessment of the fluoride-rich region in the Cu-O-F system, Thermochim. Acta 663 (2018) 194–214, doi:10.1016/j.tca.2017.11.013.
[52] E. Barsoukov, J.R. Macdonald, Impedance Spectroscopy: Theory, Experiment, and Applications, Third ed., John Wiley & Sons, Inc., Hoboken, New Jersey, 2018.
[53] K.D. Pershina, K.A. Kazdobin, Impedance spectroscopy of electrolytic materials, Education of Ukraine, Kiev, 2012.
[54] Y.K. Jeong, G.M. Choi, Nonstoichiometry and electrical conduction of CuO, J. Phys. Chem. Solids 57 (1996) 81–84, doi:10.1016/0022-3697(95)00130-1.